DOI: 10.1002/fuce.201000130

Innovative Hybrid Cycle Solid Oxide Fuel Cell-Inverted Gas Turbine with CO_2 Separation

Emanuele Facchinetti[1]*, Daniel Favrat[1], and François Marechal[1]

[1] Ecole Polytechnique Federale de Lausanne, EPFL, Lausanne, Switzerland

Received August 11, 2010; accepted May 19, 2011

Abstract

Decentralized power generation and cogeneration of heat and power is an attractive way toward a more rational conversion of fossil or biofuel. In small-scale power production fuel cell–gas turbine hybrid cycles are an emerging candidate to reach higher or comparable efficiency than large-scale power plants. The present contribution introduces an innovative concept of hybrid cycle that allows targeting high efficiency together with carbon dioxide separation and maintaining the fuel cell operating under atmospheric condition. The system consists in a planar module of solid oxide fuel cell operating at atmospheric pressure, an oxy-combustion unit, and two separated gas turbine units driven in an inverted Brayton cycle. A thermodynamic optimization approach, based on the system energy integration, is used to analyze several design options. Optimization results demonstrate that the proposed hybrid system enables higher energy conversion efficiency with respect to an equivalent state of the art pressurized hybrid system, whilst avoiding fuel cell pressurization technical problems, and enabling the carbon dioxide separation. The potential of designs achieving 80% First Law efficiency is shown.

Keywords: CO_2 separation, Gas Turbine, Hybrid Cycle, Inverted Brayton, Solid Oxide Fuel Cell

1 Introduction

The rising demand for electrical power and the necessity to decrease fossil fuel consumption push for development of new power generation systems, with higher efficiencies, and reduced environmental impacts. An attractive way to reach a more rational energy conversion of fossil or biofuels is the decentralized power generation and cogeneration of heat and power.

Among major weaknesses of existing small systems at the building level, consisting mainly of internal combustion or Stirling engines, are low electrical efficiency, high maintenance costs, together with noise and vibration. The introduction of mini gas turbines in the range of 40–120 kWel have reduced the three latter problems, however, at an even lower efficiency. Moreover they are not available in the smaller power range typical of many multi-family houses. Molten carbon fuel cells (MCFC) and solid oxide fuel cells (SOFC) are emerging as major candidates to alleviate all the above-mentioned drawbacks. However, the fuel cannot be entirely converted electrochemically in the fuel cell alone and part of it is combusted downstream of the fuel cell with a low energy efficiency. Several existing approaches suggest to further improve the electrical efficiency by combining the fuel cell with other conventional thermal cycles in a hybrid system. The most appropriate integration strategy is defined by the application requirements. Recently Zhang et al. [1] reviewed the available SOFC-based hybrid systems. Due to the high operating temperature and to the use of a gas-based working fluid, the Brayton cycle is a favorable candidate for SOFC integration.

In the last years the research demonstrated the potential and limits of this technology. Many studies have assessed the feasibility and operating conditions of a variety of integrated high efficiency design options. Those alternatives are usually classified either in pressurized systems, if the fuel cell is operating under pressurized conditions, or in atmospheric systems. So far the studies showed that the pressurized systems

[*] *Corresponding author, emanuele.facchinetti@epfl.ch*

reach the highest efficiencies. Palsson et al. [2] showed the possibility to reach in a pressurized system, also with a low pressure ratio, more than 65% of efficiency. Massardo and Lubelli [3] analyzed pressurized and atmospheric systems with efficiencies up to 75%. Park and Kim [4] assessed the higher performance of a pressurized system with respect to a comparable indirectly heated atmospheric system. Autissier et al. [5] performed a thermoeconomic analysis demonstrating the possibility to reach 70% efficiency for an estimated 6,700 \$ kW^{-1} with a 50 kW pressurized system. Tsujikawa et al. [6,7] proposed an interesting way to fully integrate a gas turbine driven in an inverted Brayton cycle with a fuel cell operating under atmospheric conditions. The inverted Brayton cycle, which has been fully detailed by Wilson [8], is characterized by the expansion in the turbine before the compression.

Given the need to reduce carbon dioxide emissions, several studies have aimed at assessing the performance of hybrid systems integrating carbon dioxide separation technologies. Franzoni et al. [9] compared the thermoeconomic performance of the carbon dioxide capture in a pressurized system via chemical absorption and via oxy-fuel combustion. Park et al. [10] demonstrated the possibility to achieve system efficiency comparable to an equivalent pressurized system but enabling carbon dioxide separation via oxy-fuel combustion.

Despite the high potential, so far the experimental applications of fully integrated highly efficient hybrid systems remain limited to a small number of cases. The World's first demonstration of the SOFC-gas turbine hybrid concept, including a pressurized tubular SOFC module integrated with a microgas turbine, was delivered to Southern California Edison for operation at the Irvine's National Fuel Cell Research Center. This system reached 53% electric efficiency for 220 kW [11]. A few other experimental applications have been developed, but all are restricted to the bulky tubular SOFC stacks. SOFCs are available in two different typologies: tubular geometry and planar geometry. The latter are more effective, compact, and globally less material intensive than the tubular geometry based, but even more challenging to operate under pressurized conditions. Only recently, Lim et al. [12] operated for a few hours a pressurized hybrid cycle with a 25 kW microgas turbine and a 5 kW class planar SOFC, originally designed to work under atmospheric conditions.

So far the fuel cell pressurization remains a major challenge to overcome and represents a limit to the hybrid cycle development. The present paper introduces an innovative concept of atmospheric hybrid cycle combined with oxy-fuel combustion technology capable of reaching efficiencies higher or comparable to the state of the art, whilst avoiding fuel cell pressurization and enabling the carbon dioxide separation [13]. The system consists in a planar module of SOFC operating at atmospheric pressure, an oxy-combustion unit and two separated gas turbine units driven in an inverted Brayton cycle. A thermodynamic optimization approach, coupled with the system energy integration, is used to compare the proposed system with an equivalent state of the art pressurized hybrid cycle. The optimal system designs are presented and compared on the basis of First Law and exergy analyses.

2 System and Model Description

An innovative concept of SOFC-gas turbine hybrid cycle is introduced, described, and compared with the state of the art hybrid cycle. The developed system model is detailed underneath.

2.1 *Innovative Hybrid Cycle*

The concept is based on a planar SOFC operating at atmospheric pressure integrated with two gas turbines driven in an inverted Brayton cycle and including oxy-fuel combustion. One embodiment of the system is presented in Scheme 1.

The idea is to capitalize on the intrinsic oxygen–nitrogen separation characteristic of the fuel cell electrolyte by expanding in separate gas turbines the cathodic flow and the anodic

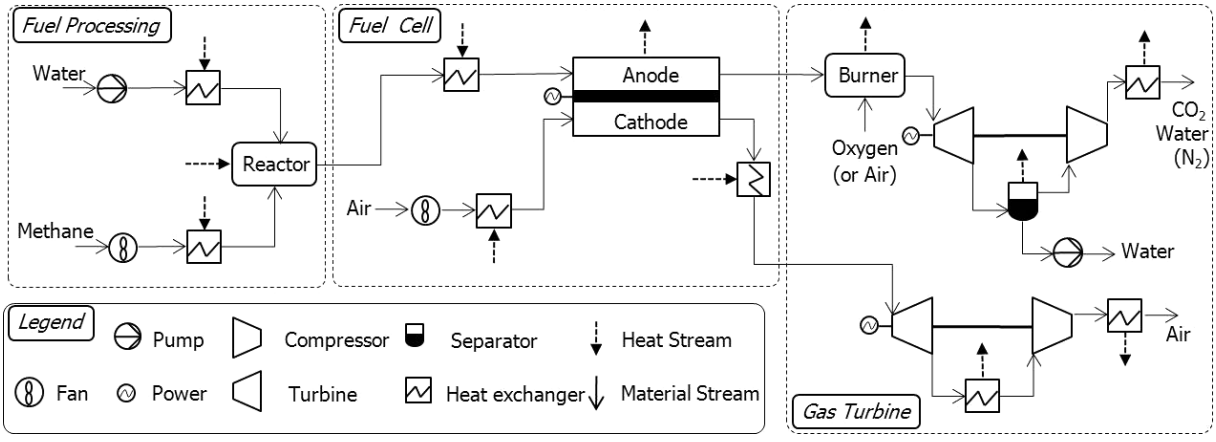

Scheme 1 Innovative hybrid cycle flow-chart.

flow, the latter being free of nitrogen. The cathodic flow, consisting in air impoverished in oxygen at the fuel cell outlet temperature, could be additionally heated up before being expanded in the sub-atmospheric gas turbine. The anodic flow coming out of the fuel cell contains a part of unconverted fuel depending on the fuel utilization factor of the fuel cell. This remaining fuel is oxidized in a combustion chamber. If the oxidizer used is pure oxygen, the anodic flow passing through the turbine consists of only carbon dioxide and water. Water can easily be condensed and separated in a cooling heat exchanger positioned between the turbine and the compressor. The compressor mainly compresses carbon dioxide to the atmospheric pressure, whereas, water is pumped up separately. Carbon dioxide, available at atmospheric pressure, can be stored for other uses or can be further compressed to a compatible state for transportation and sequestration. As gas compression is much more demanding in terms of mechanical power than liquid pumping, the reduced gas flow leads to savings of power with respect to traditional systems. To benefit as much as possible from this gain, supplementary steam can be injected in the fuel processing unit. As a consequence, the anodic flow steam injection rate is another degree of freedom and is usually increased in comparison with standard hybrid fuel cell-gas turbine systems.

The advantages of carbon dioxide separation and compressor power reduction, although reduced, are maintained when the post combustion is realized with air instead of pure oxygen. This is due to the fact that post combustion concerns only a small part of the total fuel conversion in the system. In this case carbon dioxide and nitrogen have to be recompressed and separated afterwards if carbon dioxide capture and storage is required. Analyses have been performed on both cases, with pure oxygen injection and with air injection.

Since the innovative concept can be applied in any range of power, the system analysis performed is size independent.

2.2 Model Description

A steady-state model of the new hybrid cycle concept has been developed. The system model is subdivided into three sub-systems: fuel processing, fuel cell, and gas turbines. Each sub-system includes an energy flow model computing the thermodynamic performance and the energy requirement. The models have been developed using a commercial process modeling software, BELSIM-VALI [14].

2.2.1 Fuel Processing

To simplify, the fuel feeding the system is methane, which is the major component of natural gas or of some biogas. The fuel processing is based on steam reforming, which can partially be internal. An appropriate excess of steam is guaranteed to avoid the formation of soot, which is an important cause of degradation. A carbon deposition risk model has been developed and integrated into the energy model. Pressure drops are neglected. The auxiliary devices needed, including pumps and blowers, are driven by the electrical power provided by the system.

2.2.2 Fuel Cell

The partially reformed fuel coming from the fuel processing unit feeds the anode of a planar SOFC operating under atmospheric pressure. Although not necessary in steady-state operation, a blower, electrically driven by the system, provides the required airflow to the cathode.

The fuel cell model is based on the model for planar technology developed by Van herle et al. [15]. Anode supported cells, composite LSCF cathode, and metallic interconnectors are assumed. The electrochemical model includes diffusion losses at the anode and cathode, as well as other polarization and ohmic losses. Possibility of internal reforming is included. The cell potential is a function of inlet gases composition, current density, and fuel utilization. Since the approach used does not consider any constraints on the fuel cell size, the current density has been considered fixed to 0.3 A cm^{-2}. The inlet temperature is limited in the range between 973 and 1,073 K. To avoid cracks, the temperature difference across the stack is maintained below 100 K by removing the eventual extra energy through a heat exchanger. Pressure drops are neglected.

The model has been calibrated using experimental results presented by Wuillemin [16].

2.2.3 Gas Turbines

The anodic flow coming out the SOFC is mixed with an oxidizer in the combustion chamber in order to realize a stoichiometric and complete combustion. Post combustion hot gases have to be cooled down to the turbine inlet temperature (TIT).

Considering the characteristic of the system and the size-independent aspect of the analysis, the parameters characterizing the turbomachinery have been chosen so as to cover applications in different power ranges. The isentropic efficiency is supposed constant and equal to 0.85. Pressure drops are neglected. The analysis is performed for two different TIT limits: 1,173 and 1,573 K. Considering small-scale applications, in which turbine cooling systems are not feasible, 1,173 K represents a conservative TIT limit for metallic turbine, whereas, 1,573 K represents the TIT limit for ceramic turbine. In large-scale applications, in which turbine cooling system can be implemented, 1,573 K represents a conservative TIT limit.

2.3 State of the Art Hybrid Cycle

A flow-chart of a state of the art hybrid cycle, used as reference, is presented in Scheme 2. The system is based on a pressurized planar SOFC coupled with a gas turbine. A fuel processing unit, analog to the one described for the new layout, feeds the anode with partially reformed methane at the operating pressure. A compressor supplies compressed air at the cathode. The cathode and the anode flows are combined downstream of the SOFC. This mixture is sent to the combus-

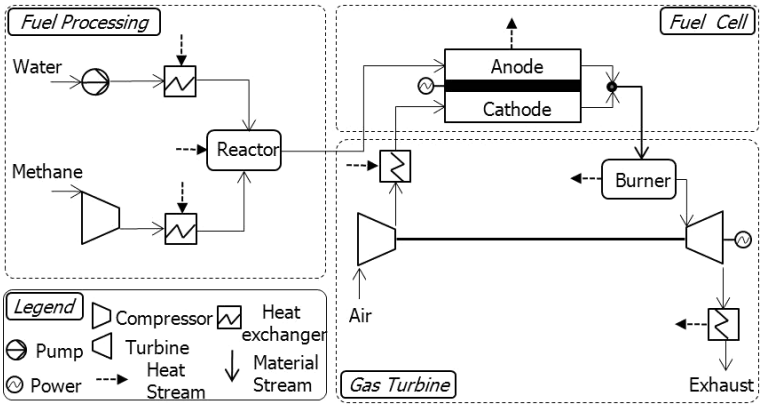

Scheme 2 State of the art hybrid cycle flow-chart.

tion chamber where the unconsumed fuel is completely oxidized. Following this, the hot gases expand in the turbine and are ejected as exhaust gases.

The models of each sub-system correspond to the model descriptions concerning the new system mentioned previously.

3 Thermodynamic Optimization

A thermodynamic optimization approach is used to evaluate several design options. The methodology consists in two phases: to model the system defining a set of decision variables and to optimize their values. This approach, described hereafter, is integrated into OSMOSE [17], a software platform for design and optimization of integrated energy systems.

3.1 System Modeling

The aim of the system modeling is to represent the impact of the design choices on the performances. The system's state and performances are expressed by variables divided in two categories: the decision variables provided as input, and the dependant variables computed as output. The system modeling is organized in three sub-models (Scheme 3): the energy flow model, the heat and power integration model, and the performance evaluation model. The energy flow model has been previously introduced and detailed in Section 2.2.

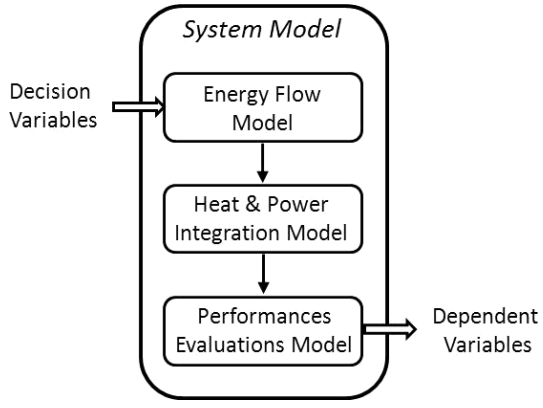

Scheme 3 System model layout.

The heat and power integration model solves the heat cascade and the energy balance of the plant maximizing the combined production of heat and power. This identifies the minimum energy requirement and sets the basis for the heat exchanger network design, based on the exergy losses minimization. The heat exchange is assumed with a pinch temperature difference (ΔT_{min}) of 10 K.

The performance evaluation model allows evaluating the system performances taking into account the energy flow model and the energy integration results. First Law efficiency and exergy efficiency are both estimated. The First Law efficiency (1) is defined as the ratio between the electrical power output and the transformation energy received by the system as input, consisting in fuel and, if required, in separated oxygen. The electrical power output is the sum of the fuel cell power output, $\dot{E}^-_{FC}$, and the net power output of the gas turbines (turbines power minus compressor and auxiliaries powers), $\sum \dot{E}^-_{GT}$. The energy transformation received by the system is calculated on the basis of the fuel lower heating value and considering the energetic cost of cryogenic oxygen production [18].

$$\varepsilon = \frac{\dot{E}^-_{FC} + \sum \dot{E}^-_{GT}}{\dot{M}^+_F \cdot \Delta h^0_{iF} + \dot{M}^+_{O_2} \times e_{cryO_2}} \quad (1)$$

According with the general definition and following the formalism proposed by Borel and Favrat [19] and Favrat et al. [20], the exergy efficiency is defined as the ratio between the exergy rate delivered by the system and the exergy rate received by the system. The exergy rate delivered by the system consists in the electrical power output and in the diffusion exergy of the separated carbon dioxide. The exergy rate received by the system is reduced to the transformation exergy received (2). The exergetic cost of the oxygen separation is considered equal to the ideal diffusion work of the pure component to its partial pressure in the atmosphere, which is the diffusion exergy [19]. This exergy efficiency definition represents a coherent thermodynamic indicator of the upper bound system performance.

$$\eta = \frac{\dot{E}^-_{FC} + \sum \dot{E}^-_{GT} + \dot{M}^+_{CO_2} \times e_{sCO_2}}{\dot{M}^+_F \times \Delta k^0_F + \dot{M}^+_{O_2} \times e_{sO_2}} \quad (2)$$

3.2 Optimization

The objective of the optimization is to choose the design options that maximize the system efficiency. The influence of the decision variables on the system efficiency can be also investigated.

The optimization is performed using MOO, a multi-objective optimizer which is described in ref. [21]. Evolutionary Algorithms are heuristic methods that base the optimization procedure on the exploration of the search space, thus allowing to optimize within a non-linear and non-continuous space of solutions. The search space is defined by the decision variables and their bounds. The MOO solution is a set of points in the decision variables space that define the possible trade-off between the objectives. The Pareto frontier expresses this compromise delimiting the unfeasible domain from the feasible but sub-optimal one.

4 Results

Three systems are compared in the results: the new system firstly with pure oxygen as oxidizer in the combustion chamber (HCox), and secondly with air (HCair), and the state of the art system (HCP). The decision variables and their range are presented in Table 1.

The relation between First Law efficiency, exergy efficiency, and pressure ratio is presented in the form of Pareto curves for the case of maximum TIT equal to 1,573 K in Figure 1. For HCox and HCair the pressure ratio reference is that of the anodic side. The system efficiency increases with the pressure ratio, although the increase becomes less important toward high pressure ratios. At low pressure ratios the performances of HCP are more sensitive to changes of the pressure ratio. In terms of First Law efficiency the configurations HCox and HCair are equivalent and between 1.3 and 1.7% more effective than HCP. The performance advantage with respect to HCP is due to the reduction in compression power and the lower exergy losses enabled by the new hybrid cycle concept. This gain is more important in HCox than in HCair, since by avoiding the presence of nitrogen a higher amount of water can be condensed and pumped up, and compensates the penalty due to the pure oxygen separation required by the oxy-combustion characteristic of HCox.

Table 1 Decision variables.

Variables	Range	Variables	Range
ξ_{sc}	[0.7–3.5]	μ	[0.6–0.8]
T_{sr} [K]	[973–1,073]	π	[2.5–6]
T_{fc} [K]	[973–1,073]	T_{ic} [K]	[298–343]
λ	[2–10]	TIT_{max} [K]	[1,173 or 1,573]

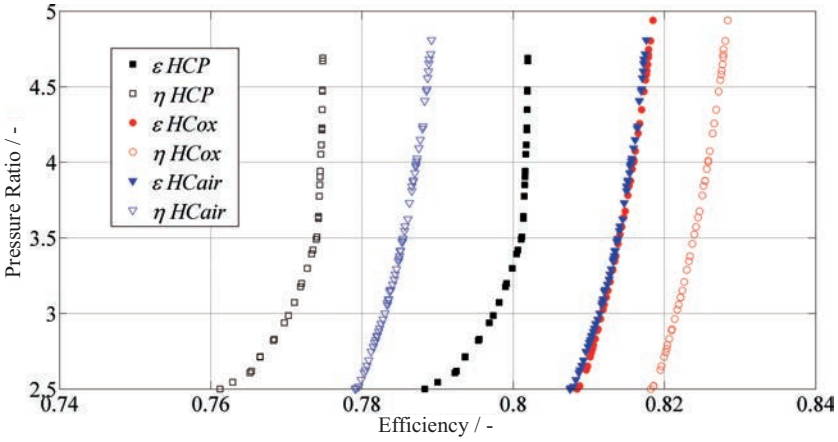

Fig. 1 Efficiency *vs.* pressure ratio with max TIT = 1,573 K.

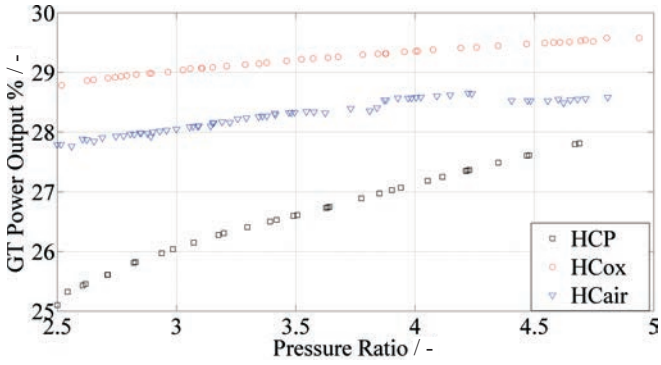

Fig. 2 Pressure ratio *vs.* gas turbines power output percentage with max TIT = 1,573 K.

However, the First Law efficiency does not consider the carbon dioxide separation value and in general is not an exhaustive indicator of energy conversion performance. The exergy efficiency is the most appropriate performance indicator to estimate the thermodynamic quality of an energy conversion system. In terms of exergy analysis HCox is the most performing system: the analysis proves that HCox is about 3.9% more effective than HCair and around 5.2% more effective than HCP.

Figure 2 illustrates how the system power output is distributed between the gas turbines and the fuel cell. Since the fuel cell allows a more efficient energy conversion compared to the gas turbine the fuel cell fuel utilization is always maximized to the upper limit of its allowable range and the gas turbines power output is limited between 25 and 30% of the total power output. The reduced compression work enables HCox to have the highest rate of power supplied by the gas turbines.

For all configurations the optimization leads to a high fuel cell inlet temperature, which increases the fuel cell performance, and to a high steam reforming temperature, which promotes the hydrogen conversion enabling to keep the steam to carbon ratio in a lower range, as required by energy integration constraints. Figure 3 shows the relation between the steam to carbon ratio and the pressure ratio. As the risk of carbon deposition increases with pressure, the optimal steam to carbon ratio of HCP increases with the pressure ratio and is larger than for HCox and HCair. A larger steam to carbon ratio means more steam passing through the

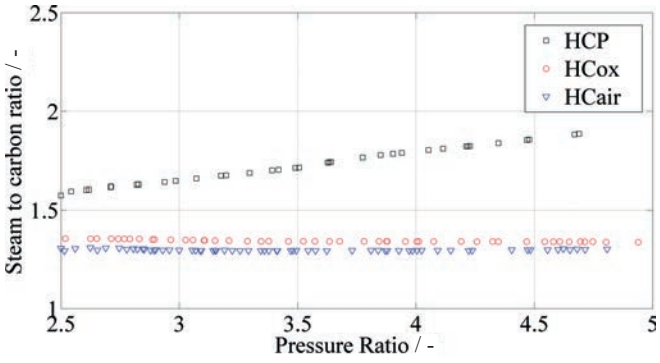

Fig. 3 Pressure ratio *vs.* steam to carbon ratio with max TIT = 1,573 K.

fuel cell and thus reduced fuel cell cooling requirement. Indeed, the optimal HCP fuel cell air excess decreases with the pressure ratio (Figure 4). HCox and HCair are characterized by a nearly constant steam to carbon ratio and fuel cell air excess.

The cathodic turbine pressure ratio remains nearly constant for HCox while decreases slightly for HCair with respect to the anodic pressure ratio (Figure 5).

Figure 6 displays the relation between the pressure ratio and the anodic and cathodic compressor inlet temperatures. Anodic and cathodic compressor inlet temperatures of HCair

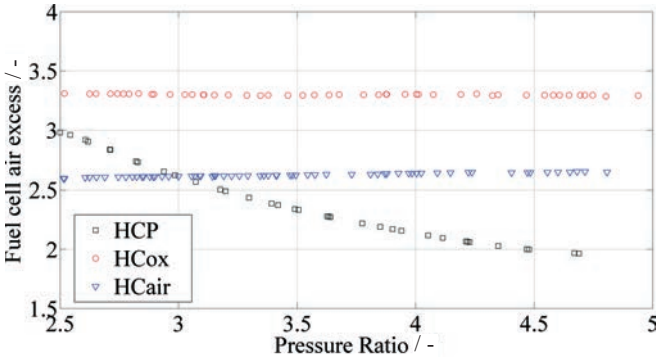

Fig. 4 Pressure ratio *vs.* fuel cell air excess with max TIT = 1,573 K.

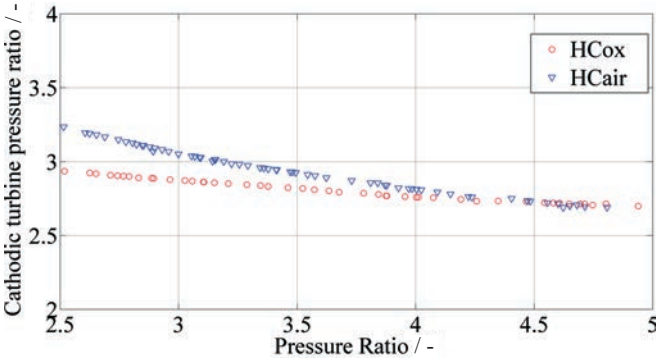

Fig. 5 Pressure ratio *vs.* cathodic turbine pressure ratio with max TIT = 1,573 K.

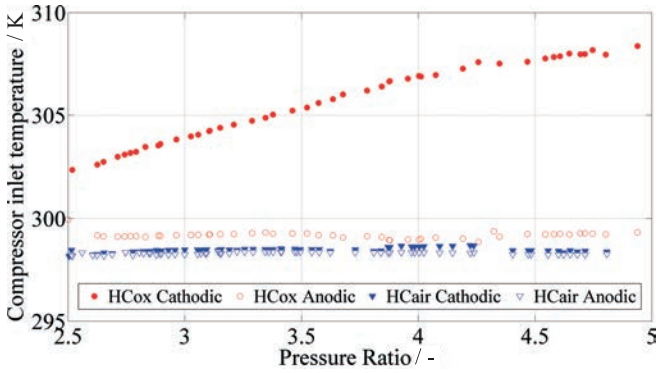

Fig. 6 Pressure ratio *vs.* compressor inlet temperature with max TIT = 1,573 K.

are minimized in order to reduce the compression work. The compressor inlet temperatures of HCox are slightly higher than the lower limit of the range. This is due to the low temperature heat load required by the system energy integration.

Corrected composite curves of optimal solutions, characterized by the same pressure ratio, are compared in Figures 7–9. The decision variables describing those solutions are presented in Table 2. The corrected composite curves represent the relation between corrected temperature $(T \pm (\Delta T_{min}/2))$ and the heat load specific to the power output.

Table 2 Decision variables for optimal solutions $\pi = 3$ and max TIT = 1,573 K.

Variables	HCox	HCair	HCP
ξ_{sc}	1.35	1.30	1.65
T_{sr} [K]	1,065	1,073	1,071
T_{fc} [K]	1,072	1,073	1,073
λ	3.3	2.6	2.6
μ	0.8	0.8	0.8
π	3	3	3
$\pi_{cathode}$	2.9	3.0	–
$T_{ic\ cathode}$ [K]	299	298	–
$T_{ic\ anode}$ [K]	304	298	–

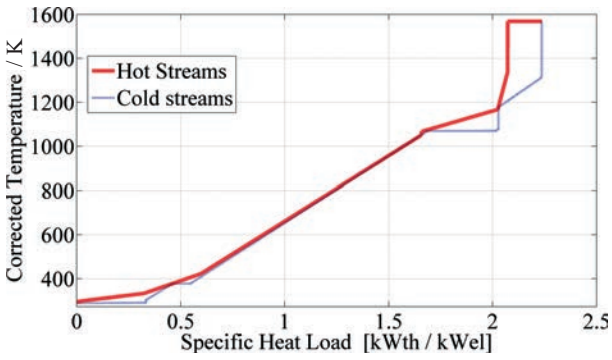

Fig. 7 HCox composite curves of optimal solution with $\pi = 3$ and max TIT = 1,573 K.

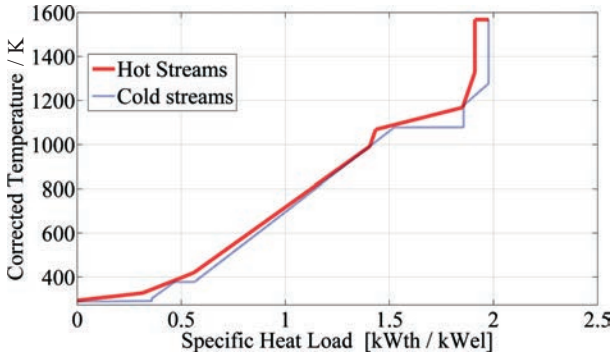

Fig. 8 HCair composite curves of optimal solution with $\pi = 3$ and max TIT = 1,573 K.

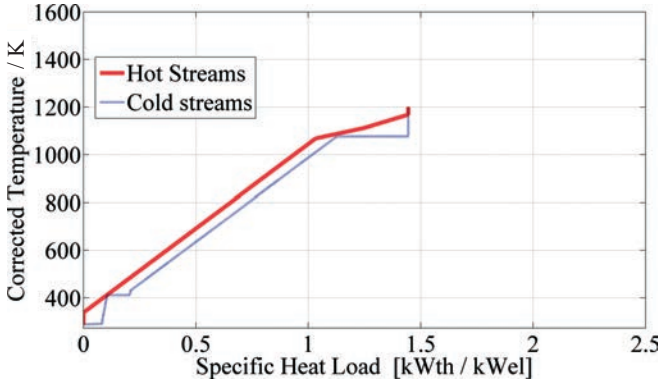

Fig. 9 HCP composite curves of optimal solution with $\pi = 3$ and max TIT = 1,573 K.

The cold curve represents the heat requirements of the cooling water utility, the water and the fuel supplied to the fuel process unit, the air provided to the cathode, and the steam reforming reactor. The hot curve represents the heat extracted to limit the TIT, to cool down the fuel cell and the turbine outlets.

Three pinch points are created in HCox and HCair: at low temperature by the steam production for the fuel processing, at intermediate temperature by the steam reforming, and at high temperature by the additional heating of the cathodic turbine inlet. HCP has only the pinch point at low temperature created by the steam production.

The heat load of the two atmospheric systems is higher with respect to that of the pressurized system. Two elements contribute to explain this difference: the water condensation in HCox and HCair and the different air excess in the fuel cell. An important amount of heat is extracted in the low temperature zone of HCox and HCair for the water condensation in the anodic flow. The largest part of this heat is evacuated by the cooling water utility. In HCP the water is evacuated as steam in the exhaust gases. The

Table 3 Decision variables for optimal solutions $\pi = 3$ and max TIT = 1,173 K.

Variables	HCox	HCair	HCP
ξ_{sc}	1.31	1.31	1.65
T_{sr} [K]	1,071	1,073	1,072
T_{fc} [K]	1,072	1,073	1,073
λ	4.4	3.6	3.1
μ	0.8	0.8	0.8
π	3	3	3
$\pi_{cathode}$	2.6	2.6	–
$T_{ic\ cathode}$ [K]	298	298	–
$T_{ic\ anode}$ [K]	314	299	–

different air excess explains the residual difference of the heat load: if the air excess is higher more air is heated up in the fuel processor unit and more heat is recuperated before the cathodic compressor. The heat exchanged between the incoming cold air and the outgoing hot air represents the main fraction of the heat exchanged in the intermediate temperature zone. In this region HCox and HCair are characterized by lower exergy losses with respect to HCP. The possibility to differentiate the cathodic and anodic pressure ratios enables a reduction in exergy losses, especially in this intermediate temperature zone. On the contrary in the high temperature zone, HCP has lower exergy losses. The high air excess characterizing the combustion in HCP maintains a low temperature at the turbine inlet, thus reducing the exergy losses. For the same reason the exergy losses are more significant for HCox than for HCair, in which the nitrogen injected in the combustor contributes to cool down the flow.

In conclusion, the influence of a lower TIT is investigated. The Pareto frontiers obtained considering 1,173 K as TIT limit are shown in Figure 10. The decision variables characterizing optimal solutions for $\pi = 3$ are presented in Table 3. The expected decrease in efficiency is around 1.4% for HCox, around 1% for HCair, and around 2.1% for HCP, in the whole pressure ratio range. The configurations based on the new concept are less sensitive to the TIT variation.

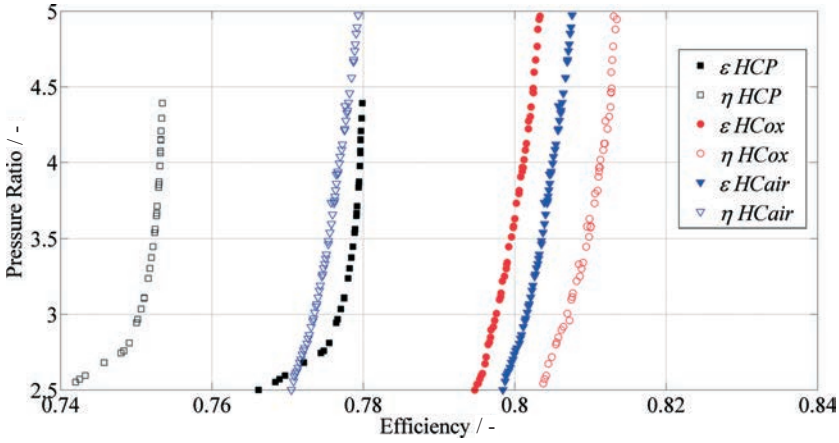

Fig. 10 Efficiency *vs.* pressure ratio with max TIT = 1,173 K.

5 Conclusion

A new concept of power generation system integrating a SOFC operating at atmospheric pressure, two gas turbine units based on an inverted Brayton cycle and oxy-fuel combustion is introduced. A model of the system has been developed. Process integration techniques have been used to investigate several design options and estimate the integrated system performance. A size-independent analysis has been carried out to compare the new system with an equivalent state of the art pressurized hybrid cycle.

Despite the more challenging system regulations and heat exchangers network definition, due to the integration of two gas turbines, the advantages offered by the innovative hybrid cycle with respect to the state of the art, are substantial.

The proposed hybrid system enables higher energy conversion efficiency, whilst avoiding fuel cell pressurization technical problems since the fuel cell operates at atmospheric pressure, and enables carbon dioxide separation, as oxy-fuel combustion is used. The thermodynamic optimization results demonstrate that the new system can achieve 80% First Law efficiency operating with a pressure ratio of 5. In terms of First Law efficiency the gain with respect the state of the art is about 1.5%. However, the value of carbon dioxide separation cannot be evaluated by the First Law efficiency. The exergy analysis proves that the gain in terms of exergy efficiency with respect to the state of the art is about 5%. Further performance improvement could be expected with an intercooled compressor of the anodic gas turbine.

List of Symbols

T_{ic}	Compressor inlet temperature / K
$()^+$	Convention positive into the system
$()^-$	Convention positive out of the system
e_{cryO_2}	Cryogenic oxygen energetic cost / kJ kg^{-1}
$\dot{E}$	Exergy of mechanical work/electricity / W
T_{fc}	Fuel cell inlet temperature / K
$\dot{M}$	Mass flow / kg s^{-1}
e_s	Specific diffusion exergy / kJ kg^{-1}
Δk^0	Specific exergy value / kJ kg^{-1}
Δh_i^0	Specific lower heating value / kJ kg^{-1}
T_{sr}	Steam reforming temperature / K

Greek Symbols

ε	First Law efficiency
λ	Fuel cell air excess
μ	Fuel cell fuel utilization
η	Exergy efficiency
π	Pressure ratio
ξ_{sc}	Steam to carbon ratio

Subscripts and Superscripts

F	Fuel
FC	Fuel cell
GT	Gas turbine

References

[1] X. Zhang, S. H. Chan, G. Li, H. K. Ho, J. Li, Z. Feng, *J. Power Sources* **2010**, *3*, 195.
[2] J. Palsson, A. Selimovic, L. Sjunnesson, *J. Power Sources* **2000**, *1*, 86.
[3] A. F. Massardo, F. Lubelli, *J. Eng. Gas Turbines Power* **2003**, *1*, 122.
[4] S. K. Park, T. S. Kim, *J. Power Sources* **2006**, *1*, 163.
[5] N. Autissier, F. Palazzi, F. Marechal, J. van Herle, D. Favrat, *J. Fuel Cell Sci. Technol*. **2007**, *2*, 4.
[6] Y. Tsujikawa, K.-I. Kaneko, J. Suzuki, *JSME Int. J. Ser. B:Fluids Therm. Eng*. **2004**, *2*, 47.
[7] Y. Tsujikawa, T. Yamauchi, K. Kaneko, S. Katsura, *Proceedings of the ASME Turbo Expo 2006* **2006**, 4.
[8] D. G. Wilson, *The Design of High-Efficiency Turbomachinery and Gas Turbines*, MIT Press, London, United Kingdom, **1993**, 135.
[9] A. Franzoni, L. Magistri, A. Traverso, A. F. Massardo, *Energy* **2008**, *2*, 33.
[10] S. K. Park, T. S. Kim, J. L. Sohn, Y. D. Lee, *Appl. Energy* **2011**, *4*, 88.
[11] S. E. Vejo, L. A. Shockling, J. T. Dederer, J. E. Gillet, W. L. Lundberg, *J. Eng. Gas Turbines Power* **2002**, *4*, 124.
[12] T.-H. Lim, R.-H. Song, D.-R. Shin, J.-I. Yang, H. Jung, I. C. Vinke, S.-S. Yang, *Int. J. Hydrogen Energy* **2008**, *3*, 33.
[13] E. Facchinetti, D. Favrat, F. Marechal, *International Patent Application, WO 2011/001311 A2*, **2011**.
[14] S. A. Belsim, VALI IV, www.belsim.com, **2009**.
[15] J. Van Herle, F. Maréchal, S. Leuenberger, D. Favrat, *J. Power Sources* **2003**, *1*, 118.
[16] Z. Wuillemin, *PhD Thesis*, Ecole Polytechnique Federale de Lausanne, Switzerland, **2009**.
[17] F. Marechal, D. Favrat, F. Palazzi, J. Godat, *J. Fuel Cells* **2004**, *1*, 5.
[18] C. Hamelinck, A. Faaij, H. Denuil, H. Boerrigter, *Energy* **2004**, *11*, 29.
[19] L. Borel, D. Favrat, *Thermodynamic and Energy System Analysis*, EPFL Press, Lausanne, Switzerland **2010**, 399.
[20] D. Favrat, F. Marechal, O. Epelly, *Energy* **2008**, *2*, 33.
[21] A. Molyneaux, G. Leyland, D. Favrat, *Energy* **2010**, *2*, 35.

